relationships that led to the eventual domestication of weedy annuals in eastern North America.

REFERENCES AND NOTES

1. B. D. Smith, in *Advances In World Archaeology*, F. Wendorf and A. Close, Eds. (Academic Press, New York, 1986), vol. 5, pp. 1–92.
2. J. A. Ford, *Science* **122**, 550 (1955).
3. J. L. Gibson, in *Archaeology of the Mid-Holocene Southeast*, K. E. Sassaman and D. G. Anderson, Eds. (Univ. of Florida Press, Gainesville, FL, 1996), pp. 288–305.
4. J. L. Gibson and J. R. Shenkel, in *Middle Woodland Settlement and Ceremonialism in the Mid-South and Lower Mississippi Valley*, R. C. Mainfort Jr., Ed. (Archaeological Report No. 22, Mississippi Department of Archives and History, Jackson, MS, 1988) pp. 7–18.
5. M. Russo, *Southeast. Archaeol.* **13**, 93 (1994).
6. J. W. Saunders and T. Allen, *Am. Antiq.* **59**, 471 (1994).
7. _____, R. T. Saucier, *Southeast. Archaeol.* **13**, 134 (1994).
8. M. Russo, in *Archaeology of the Mid-Holocene Southeast*, K. E. Sassaman and D. G. Anderson, Eds. (Univ. of Florida Press, Gainesville, FL, 1996), pp. 259–287.
9. R. T. Saucier and A. R. Fleetwood, *Geol. Soc. Am. Bull.* **81**, 869 (1970).
10. R. T. Saucier, *Geomorphology and Quaternary Geologic History of the Lower Mississippi Valley* (U.S. Army Engineer Waterways Experiment Station, Vicksburg, MS, 1994), vol. I.
11. Ridge B/C is the exception.
12. P. W. Birkeland, *Soils and Geomorphology* (Oxford Univ. Press, New York, 1984).
13. Charcoal from the mound D submound surface dated to 3824 ± 120 cal. calendar years B.P. (β95003). Humate ages from the same horizon and buried A horizons above the sample were >700 years older. Charred bone from augering of stage I, mound B dated to 4140 ± 60 cal. calendar years B.P. (β72331). Subsequent charcoal samples from mound B, stage I and overlying stage II were 1000 years older.
14. C. W. Martin and W. C. Johnson, *Quat. Res.* **43**, 232 (1995).
15. Y. Wang, R. Amundson, S. Trumbore, *ibid.* **45**, 282 (1996).
16. J. K. Feathers, *Quat. Geochronol.* **16**, 333 (1997).
17. G. A. T. Duller, *Radiat. Meas.* **24**, 217 (1995).
18. D. S. Frink, in *Pedological Perspectives in Archaeological Research*, M. Collins, Ed. (Soil Science Society of America Special Publication 44, Madison, WI, 1995).
19. _____, *Archaeol. East. North Am.* **20**, 67 (1992).
20. C. H. Webb, "The Poverty Point Culture" No. 17 (School of Geoscience, Louisiana State University, Baton Rouge, LA, 1982).
21. A Poverty Point Object was found in level 1, TU 7, ridge B/C.
22. F. Schambach, thesis, Harvard University (1970).
23. M. D. Jeter and H. E. Jackson, *La. Archaeol.* **17**, 133 (1994).
24. J. L. Gibson, *ibid.*, p. 251.
25. C. H. Webb and J. L. Gibson, *Geosci. Man* **22**, 85 (1981).
26. J. L. Gibson, *Bull. Tex. Archaeol. Soc.* **38**, 1 (1968).
27. J. Connaway, *La. Archaeol.* **8**, 57 (1981).
28. J. K. Johnson, *Southeast. Archaeol.* **12**, 59 (1993).
29. B. D. Smith, *Rivers of Change: Essays on Early Agriculture in Eastern North America* (Smithsonian Institution Press, Washington, DC, 1993).
30. M. Stuiver and P. M. Reimer, Radiocarbon Calibration Program 1993, rev. 3.0.3c (Quaternary Isotope Lab, University of Washington, Seattle, WA).
31. Funders included the National Geographic Society (two grants), the National Park Service, and the State of Louisiana. The Gentry family, Willamette Industries, Inc., and the Archaeological Conservancy allowed access to the site.

27 May 1997; accepted 4 August 1997

Reversible Nanocontraction and Dilatation in a Solid Induced by Polarized Light

P. Krecmer, A. M. Moulin, R. J. Stephenson, T. Rayment, M. E. Welland, S. R. Elliott*

Reversible, controllable optical nanocontraction and dilatation in a chalcogenide glass film was induced by polarized light, and a direct correlation of this optomechanical effect with the reversible optical-induced optical anisotropy (dichroism) also exhibited by the chalcogenide glass was observed. A microscopic model of the photoinduced, reversible structural phenomenon responsible for the optomechanical behavior is presented. The ability to induce an anisotropic optomechanical effect could form the basis of a number of applications, including polarized light-dependent optical nanoactuators, optomechanical diaphragm micropumps, and even motors driven by polarized light.

So far, only piezoelectric and electrostrictive positioning devices have the potential to meet the accuracy demands in nanotechnology, which require movement and measurement with nanometer-scale precision (*1*). Here we show that certain amorphous semiconducting materials exhibit an optomechanical effect that is solely dependent on the absorption of polarized light. This effect could be exploited to make devices that would supplement or substitute the presently available range of electric field–dependent piezoelectric devices.

Reversible photoinduced anisotropy (PA) can be induced by polarized light (so-called vectoral phenomenon) in chalcogenide glasses (*2*, *3*). By using this effect, a previously optically isotropic chalcogenide glass sample can be made linearly or circularly dichroic or birefringent after the absorption of linearly or circularly polarized light, respectively. Current views on the structural origin of PA can be classified into two groups. The first group ascribes PA to a variety of relatively isolated atomic events that occur at short length scales, mainly on the basis of the spatial redistribution of covalent bonds (*2*), directional changes in the electric dipole moment arising from defect sites (*4*), or lone-pair electron orbitals (*5*) inherent in chalcogenide glasses. The second group invokes the orientation of structural elements that interact at longer length scales, that is, pseudocrystal-like structures (*6*), or the cooperative effect of local anisotropic events resulting in a global distortion of the amorphous network (*5*).

Our investigations show that upon irradiation with polarized light, thin amorphous films of $As_{50}Se_{50}$ exhibit reversible nanocontraction parallel to the direction of the electric vector of the polarized light and nanodilatation along the axis orthogonal to the electric vector of the light. This behavior can be interpreted in terms of a network-related mechanism for this reversible optomechanical and PA effect.

A direct method for the determination of stress in thin films involves the bending of a microbeam (cantilever), in which a change in the stress of a film deposited on one side will cause the film-cantilever structure to bend to minimize its stored strain energy. If, for instance, the tensile stress in the film deposited on the top surface of the cantilever increases, the film tends to contract and the cantilever bends up.

We focused a probe laser onto the end of a cantilever and measured the bending of the beam by the movement of the reflected laser spot on a position-sensitive photodiode; the deflection of the cantilever is linearly dependent on the current output. We used commercially available V-shaped atomic force microscope microcantilevers. They are fabricated from silicon nitride with typical dimensions of 200 μm in length, 20 μm in width, and 0.6 μm in thickness, and the bottom surface is coated with a thin layer of gold (~20 nm thick) that increases the optical reflectivity for the probe laser beam. A thin amorphous $As_{50}Se_{50}$ film (250 nm thick) was evaporated on to the top surface of the cantilever. As demonstrated previously (*7*, *8*), a composite cantilever is sensitive to thermal changes, for example, when heated by another laser beam incident on the top surface. This phenomenon, the bimetallic effect, results from the differential thermal expansion of the two bonded materials. The total stress change in a deposited film is therefore the sum of two components: the internal and thermal stresses. The internal stress is related to differences in the structure, which, for this experiment, was modified by a change in polarization of the light

---

P. Krecmer, T. Rayment, S. R. Elliott, Department of Chemistry, University of Cambridge, Lensfield Road, Cambridge CB2 1EW, UK.
A. M. Moulin, R. J. Stephenson, M. E. Welland, Department of Engineering, University of Cambridge, Trumpington Street, Cambridge CB2 1PZ, UK.

*To whom correspondence should be addressed.

incident on the chalcogenide film. To differentiate between these two types of stress, we periodically chopped the illuminating pump laser beam and recorded the ac and dc components of the measured signal separately. The synchronous response of the cantilever to thermal fluctuations is very fast [less than 1 ms in air (8)]. The amplitude of the resulting signal is proportional to the power effectively absorbed by the sensor. The latter was checked to be constant throughout the experiment. The recorded dc signal represents the changes in internal stress, which occur much more slowly than the response to thermal variations.

Microcantilevers were mounted onto the head of an atomic force microscope (Fig. 1). The film was illuminated with a He-Ne laser beam, square-wave modulated at about 50 Hz by an acousto-optic modulator (AOM), and then polarized by an electro-optic modulator (EOM). The polarized light was guided through a polarization-preserving fiber that was positioned to illuminate the whole top chalcogenide surface of the cantilever. The typical polarization ratio at the output of the fiber was 1:50. The EOM allowed the transmission of one of two orthogonal polarization planes, or a combination of both alternating at 1 kHz ("unpolarized" light). One polarization direction was chosen to be along the longitudinal axis of the cantilever, and the other direction was orthogonal to it. From Stoney's formula for the induced stress in a layer (*9, 10*) and with our detection arrangement, the stress change $\Delta\sigma$ in the $As_{50}Se_{50}$ film is given by

$$\Delta\sigma = \frac{E_s t_s l}{24(1 - \nu_s) t_f\, dLR}\, \Delta \left[\frac{i_B - i_A}{i_B + i_A}\right] \qquad (1)$$

where t is the thickness, E is Young's modulus, ν is Poisson's ratio, L is the length of the cantilever, R is the radius of curvature of the bent cantilever, and the subscripts s and f refer to the substrate and film layers, respectively; i_A and i_B are the currents measured by the linear photodiode from the two ends of the detector, l is the length of the photodiode, and d is the distance between the cantilever and the photodiode. For bulk amorphous silicon nitride, the material composing the cantilever, $E_s = 1.5 \times 10^{11}$ N/m^2 and $\nu_s = 0.3$. The presence of the normalizing term $i_A + i_B$ in the denominator means that any changes in the reflectivity of the lever surface will not contribute to errors in the calculated stress changes. This method only measures changes in stress (here due to changes in the polarization of the illuminating light) rather than absolute stress, because there is no reference point of known stress. A detailed description of the experimental set-up for the measurement of PA is given elsewhere (*4*).

Illumination of a previously isotropic sample with light of any polarization increases the compressive stress and hence induces a significant expansion of the glassy chalcogenide layer. Saturation of this scalar behavior was reached after 1 hour. Experiments with different polarizations of light were then conducted on the sample. Irradiation with polarized light oriented along the axis of the cantilever (the *y* axis, $\mathbf{E}_y$) led to a deflection of the cantilever in the $+z$ axis direction (Figs. 2, A and B, and 3A); in other words, light polarized in the $\mathbf{E}_y$ direction caused a contraction of the glass matrix. The opposite effect, that is, bending of the cantilever in the $-z$ direction involving a dilatation of the glass matrix (Figs. 2, A and B, and 3B), was observed when the light was polarized orthogonally (along the *x* axis, $\mathbf{E}_x$) to the direction of the cantilever axis. The induced stress in the film upon changing from unpolarized to polarized light of either the $\mathbf{E}_x$ or $\mathbf{E}_y$ orientation had a comparable magnitude (10^5 Pa) but opposite sign. This stress gave rise to a macroscopic contraction or dilatation of the glassy matrix from the equilibrium value, resulting from the scalar effect, of about 1 nm for a 200-μm-long cantilever. When the polarizations were alternated (Fig. 2B), the same phenomenon occurred, and the stress induced by changing the polarization from one to another was twice that observed when changing between one specific polarization and unpolarized light. The reorientation of induced stress was highly reproducible and the amplitude of such reorientation cycles remained constant even during many hours of prolonged irradiation.

Given the shape and dimensions of the cantilever, it is clear that the method is predominantly sensitive to stress changes in the direction of the longitudinal axis of the cantilever. Thus, one simple macroscopic explanation for the effect is that only one polarization of light causes the stress observed experimentally, whereas the other polarization allows the cantilever to bend the other way as it relaxes from the stressed state induced by the original polarization. This would explain the 1:1 ratio observed in Fig. 2, A and B, between the stresses caused by alternating the direction of polarization, and the 2:1 ratio between the stresses induced by switching from one polarization to the other (Fig. 2B) and that induced by alternating polarized and unpolarized light (Fig. 2A).

Cycles of alternation of light extinction and illumination with differently polarized light (Fig. 2C) show that scalar effects (fast kinetics) result in an expansion of the layer in the *x* direction. Vectoral effects are superposed on the latter effect (slower kinetics), and a contraction or an expansion of the layer (top and bottom curves) as a result of a specific polarization is observed.

The simple explanation given above has some limitations here, because, for example, the reproducible overshoot between the first (fast kinetics) and the second (slow kinetics) parts of the bottom curve of Fig. 2C can clearly be interpreted as the effect of

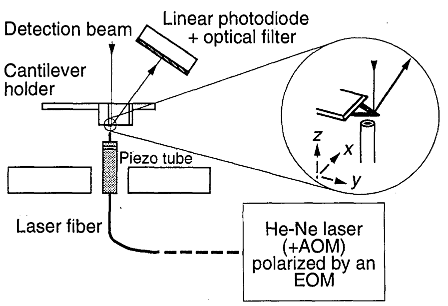

Fig. 1. Experimental set-up to measure optomechanical effects.

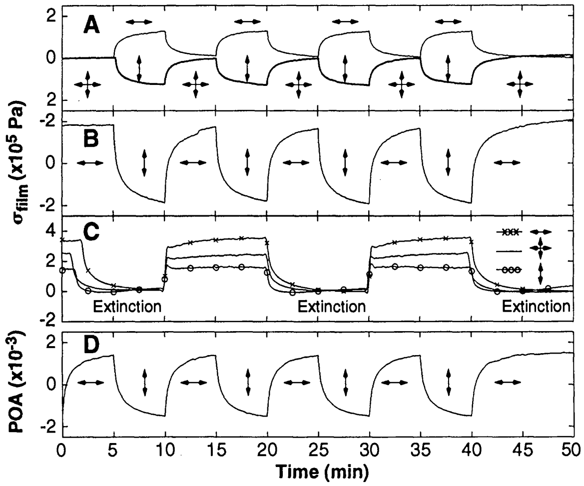

Fig. 2. Stress (σ_{film}) and photoinduced optical-anisotropy (POA) in the $As_{50}Se_{50}$ film caused by different illuminations. The vertical and horizontal arrows denote linearly polarized light and the four-pointed arrow denotes effectively unpolarized light. The "zero" stress is arbitrary because the technique measures stress variations rather than absolute stress. (**A**) Unpolarized and polarized light (in two orthogonal directions) were alternated. (**B**) Orthogonal polarizations were alternated. Note that the difference of induced stress is twice that in (A). (**C**) Different growth kinetics of photoinduced stress from the stress-free state (light extinguished) caused by a superposition of scalar and vectoral effects. (**D**) Kinetics of the appearance of POA when switching between two orthogonal linear polarizations.

a vectoral contraction superposed on the quick scalar expansion. Another criticism of this simple model is the relaxation time constant of Fig. 2C, which is of the order of 1 min. From previous optical measurements (*4*), the relaxation rate from the stressed state in absence of illumination is 3 to 4 days. We therefore need to consider an alternative explanation of the observed stress changes effected by alternate polarization based on a microscopic model.

Comparison with POA (Fig. 2D) shows a direct relation between the photoinduced mechanical stress and the optical anisotropy given by the ratio $2(I_{\parallel} - I_{\perp})/(I_{\parallel} + I_{\perp})$, where $I_{\parallel}$ and $I_{\perp}$ denote the intensities of the light transmitted through the sample with orthogonal polarizations. The growth of the PA can be fitted by a stretched exponential (Kohlrausch law) $A(t) = A_0[1 - \exp-(t/\tau)^{\beta}]$, where t is time, τ is a time constant, and the exponent β lies in the range 0 to 1, depending on light intensity and temperature (*11*). Fitting the growth kinetics of both optomechanical and PA data gives the two Kohlrausch exponents β_1 and β_2, and also two time constants τ_1 and τ_2. The average values of β_1, β_2, τ_1, and τ_2 are given in Table 1. It can be seen that β_1 and β_2 are very similar, although, because of interference problems, the PA measurements were done on thicker films of $As_{50}Se_{50}$ (2 μm thick) and thus values of the time constants τ_1 and τ_2 do not correspond exactly between the optomechanical and PA measurements.

To understand these phenomena from a microscopic point of view, we recall the ideas that assigned PA to directional changes in lone-pair (LP) electron orbitals on chalcogenide atoms. It has been estimated (*5*), with a computer model for As_2S_3 with semi-empirical interatomic potentials, that upon excitation (that is, removal) of an LP electron, a prompt swing of about 5° to 10° occurs at the chalcogen atom (S), causing a twisting of two connected AsS_3 pyramids. We developed this idea further (Fig. 3). The probability for a transition $W_{m,n}$ from state ψ_n to ψ_m is given by (*12*) $W_{m,n} = (2\ \pi t/h^2)P_{mn}P^*_{mn} \cos^2 \Theta\rho(\nu_m)$, where $\rho(\nu_m)$ is the radiation density for light with frequency ν_m, $P_{mn} = \langle\psi_m\ |\mathbf{M}|\ \psi_m\rangle$, and the transition dipole $\mathbf{M} = \Sigma q_j\mathbf{r}_j$, with q_j being the charge, $\mathbf{r}_j$ the position vector, and Θ the angle between the **E** polarization vector of the light and the axis of the transition dipole **M**. We suppose that absorption of polarized light will occur when the **E** vector of the polarized light is parallel to the main axis of the triangle consisting of a triplet of As-Se-As atoms (parallel to the transition dipole **M**) (Fig. 3C). After excitation of an LP electron an electron-hole pair is created, which no longer has the spatial symmetry of the LP orbital, and because of the change of interatomic potential, this leads to a swing at the chalcogen atom by an angle $\Delta\varphi$ from its original value φ (Fig. 3E). In our model, we consider for simplicity only geminate recombination of electron-hole pairs. Thus, after recombination, the nature of the bonding returns to its original character; however, in the short time during which the plane defined by the As-Se-As atoms is twisted (excited), a small movement of the surrounding atoms could occur in the direction of the twisting to fill the resulting void. In Fig. 3E, the chalcogen atom at the position defined by the angle $\Delta\varphi$ changes position to $\varphi + \Delta\varphi$ after absorption of a photon with the electric vector polarized in the y direction ($\mathbf{E}_y$), resulting in a local contraction of the glassy network by $\Delta\varphi$ along the φ axis. Polarized light with the electric vector $\mathbf{E}_x$ induces, vice versa, a local expansion $\Delta\varphi$ of the glassy network. A proposed angular dependence of the probability $W_{m,n}$ as a function of angle φ for both $\mathbf{E}_y$ and $\mathbf{E}_x$ polarizations is shown in Fig. 3F. An angular change of the atomic position induced by polarized light with the electric vector $\mathbf{E}_y$ increases the probability of absorption for polarized light in the x direction (Fig. 3F). Thus, we suppose that changing the plane of polarization in the x and y directions redistributes particular bond arrangements that act as a "bond switch" in these microvolumes. Combined nanoexpansion and nanocontraction of these microvolumes leads to a global anisotropic change. A more quantitative approach requires computer simulations and will be given elsewhere. However, we would like to note here the spatial distribution of such microvolumes.

Before irradiation, all transition dipoles are distributed randomly with respect to each other; hence $|\mathbf{M}_x| = |\mathbf{M}_y| = |\mathbf{M}_z|$. Linearly polarized light with the electric-field vector oriented along the y axis, $\mathbf{E}_y$ (and incident in the z direction), will excite most effectively centers having the significant absorption cross section of the transition dipole **M** directed along the y axis (Fig. 3C); in contrast, when irradiated with polarized light having the electric-field vector $\mathbf{E}_x$ in the x direction, those centers most effectively excited will have the transition dipole **M** located on the x axis (Fig. 3D).

Note that only centers having a triplet of atoms As-Se-As such that both the As atoms lie along the z axis (Fig. 3, C and D) can act as a "molecular switch," with an angular swing after the absorption of polarized inducing light. In addition, we suppose that centers having a triplet of atoms As-Se-As parallel to the x-y plane are "frozen" into stable positions during the time of irradiation, with polarized light incident along the z axis, because the angular change of transition dipoles **M** in the z axis direction does not contribute to an increase of transition dipoles for orthogonal polariza-

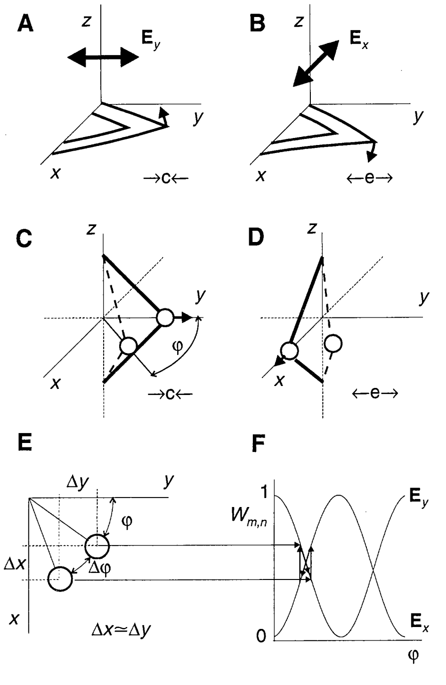

Fig. 3. (**A** and **B**) The relative orientation of the light electric vector $\mathbf{E}_{x,y}$ with respect to the cantilever. Orientation of the electric vector **E** of the inducing light parallel to the main axis of the cantilever causes contraction of the chalcogenide film (A); orientation of **E** orthogonal to the main axis of the cantilever results in expansion of the chalcogenide film (B). (**C** and **D**) Microscopic model of the swing of a chalcogenide atom after absorption of polarized light, causing (C) contraction (→c←) of a local microvolume or (D) expansion (←e→) along the y axis. (**E** and **F**) The relative angular swing of a chalcogenide atom (E) and its influence on the probability $W_{m,n}$ for $\mathbf{E}_x$ and $\mathbf{E}_y$ polarized light (F).

Table 1. Values of time constants τ_1 and τ_2 and exponents β_1 and β_2 obtained from stretched-exponential fits to the optomechanical and POA measurements.

Measurement	β_1	β_2	τ_1 (min)	τ_2 (min)
Optomechanical	0.55 ± 0.08	0.37 ± 0.04	1.0 ± 0.1	1.7 ± 0.8
Optical	0.54 ± 0.02	0.38 ± 0.04	5.1 ± 0.4	4.1 ± 0.7

tions, as reasoned above. This suggests that the ratio of the amplitudes of the induced stress should be 2:1 for illumination with light of one polarization or the other in the early stages of the measurement, before centers with triplets of As-Se-As atoms lying in the x-y plane and with the Se atoms in the y direction are "frozen" in position and no longer contribute to the overall contraction of the cantilever. Such behavior, however, could not be observed reproducibly. It is obvious that centers with an orientation of the transition dipole along the z axis are not affected by any polarized light incident along the z direction.

In the present work we have shown the possibility of reversible mechanical contraction and dilatation of an amorphous solid after the absorption of polarized light. This opto-mechanical effect may form the basis of a number of mechanical applications driven by polarized light.

REFERENCES AND NOTES

1. P. Atherton, *Laser Focus World* **30**, 107 (1994).
2. A. V. Kolobov, V. Lyubin, T. Yasuda, Ka. Tanaka, *Phys. Rev. B* **55**, 23 (1997).
3. V. M. Lyubin and V. K. Tikhomirov, *J. Non-Cryst. Solids* **114**, 133 (1989).
4. V. K. Tikhomirov and S. R. Elliott, *Phys. Rev. B* **51**, 5538 (1995).
5. J. M. Lee, M. A. Paesler, D. E. Sayers, A. Fontaine, *J. Non-Cryst. Solids* **123**, 295 (1990).
6. Ke. Tanaka, K. Ishida, N. Yoshida, *Phys. Rev. B* **54**, 9190 (1996).
7. J. R. Barnes *et al.*, *Rev. Sci. Instrum.* **65**, 3793 (1994).
8. A. M. Moulin, R. J. Stephenson, M. E. Welland, *J. Vac. Sci. Technol. B*, in press.
9. P. H. Townsend, D. M. Barnett, T. A. Brunner, *J. Appl. Phys.* **62**, 4438 (1987).
10. F. J. von Pressig, *ibid.* **66**, 4262 (1989).
11. P. Krecmer and S. R. Elliott, in preparation.
12. D. S. Kliger, J. W. Lewis, C. E. Randall, *Polarized Light in Optics and Spectroscopy* (Academic Press, New York, 1990).
13. We thank M. Frumar and M. Vlcek of the University of Pardubice for providing the facilities for making the chalcogenide films. P.K. acknowledges the Wolfson Foundation for providing financial support and A.M.M. acknowledges the financial support of the EPSRC and Unilever plc.

4 June 1997; accepted 29 July 1997

Association of Mutations in a Lysosomal Protein with Classical Late-Infantile Neuronal Ceroid Lipofuscinosis

David E. Sleat, Robert J. Donnelly, Henry Lackland,
Chang-Gong Liu, Istvan Sohar, Raju K. Pullarkat, Peter Lobel*

Classical late-infantile neuronal ceroid lipofuscinosis (LINCL) is a fatal neurodegenerative disease whose defective gene has remained elusive. A molecular basis for LINCL was determined with an approach applicable to other lysosomal storage diseases. When the mannose 6-phosphate modification of newly synthesized lysosomal enzymes was used as an affinity marker, a single protein was identified that is absent in LINCL. Sequence comparisons suggest that this protein is a pepstatin-insensitive lysosomal peptidase, and a corresponding enzymatic activity was deficient in LINCL autopsy specimens. Mutations in the gene encoding this protein were identified in LINCL patients but not in normal controls.

The neuronal ceroid lipofuscinoses (NCLs) are a group of related hereditary neurodegenerative disorders that occur at a frequency of between 2 and 4 in 100,000 live births (*1*, *2*). Most forms of NCL afflict children, and their early symptoms and disease progression tend to be similar. Diagnosis is frequently based on visual problems, behavioral changes, and seizures. Progression is reflected by a decline in mental abilities, increasingly severe and untreatable seizures, blindness, and loss of motor skills. There is no effective treatment for NCL, and all childhood forms are eventually fatal. Several forms of NCL are differentiated according to age of onset, pathology, and genetic linkage. These are infantile NCL (INCL, *CLN1*), classical late-infantile NCL (LINCL, *CLN2*), juvenile NCL (JNCL, *CLN3*), adult NCL (*CLN4*), two variant forms of LINCL (*CLN5* and *CLN6*), and possibly other atypical forms (*1*, *3*). The defective genes in INCL and JNCL have recently been identified by positional cloning (*4*, *5*), but the molecular basis for LINCL has remained elusive although the defect has recently been mapped to chromosome 11p15 (*3*). There are reasons, however, to suspect that the *CLN2* gene product could have a lysosomal function. First, LINCL, like other forms of NCL, is characterized by an accumulation of autofluorescent lysosome-like storage bodies in the neurons and other cells of patients. Second, several other related disorders are caused by lysosomal deficiencies, for example, palmitoyl protein thioesterase in INCL, neuraminidase in sialidosis, and β-hexosaminidase A in Tay-Sachs disease. Third, continuous infusion of lysosomal protease inhibitors into the brains of rats induces an accumulation of ceroid-lipofuscin in neurons that resembles NCL (*6*, *7*).

We have identified a protein that is deficient in LINCL by means of a biochemical approach that relies on the fact that newly synthesized soluble lysosomal enzymes contain a modified carbohydrate, mannose 6-phosphate (man-6-P). Man-6-P functions as a targeting signal in vivo as it is recognized by man-6-P receptors (MPRs), which direct the intracellular vesicular targeting of newly synthesized lysosomal enzymes from the Golgi to a prelysosomal compartment (*8*). Purified cation-independent MPR can be used as an affinity reagent for the detection of immobilized man-6-P glycoproteins in a protein immunoblot-style assay or can be coupled as an affinity chromatography reagent for the purification of man-6-P glycoproteins (*9*–*11*).

If LINCL results from the absence or deficiency of a lysosomal enzyme, then its corresponding man-6–phosphorylated form should also be absent or decreased. To test this possibility, we fractionated detergent-soluble extracts of LINCL patient and normal control brain autopsy samples by two-dimensional gel electrophoresis, transferred them to nitrocellulose, and detected man-6-P glycoproteins with an iodinated fragment of the MPR (Fig. 1). Normal brain contains ~75 distinct spots representing multiple isoforms of various man-6-P–containing glycoproteins (Fig. 1, top). LINCL brain is similar, except that one prominent spot is absent (Fig. 1, bottom). The corresponding normal spot is ~46 kD and has an isoelectric point (pI) of ~pH 6.0. Three other LINCL specimens were examined with the consistent observation that this protein was missing.

To identify this potential candidate for CLN2, we purified man-6-P–containing glycoproteins from normal brain by affinity chromatography on a column of immobilized MPR and, after fractionation by SDS–polyacrylamide gel electrophoresis (PAGE)

D. E. Sleat, H. Lackland, C.-G. Liu, I. Sohar, P. Lobel, Center for Advanced Biotechnology and Medicine, Piscataway, NJ 08854, USA and Department of Pharmacology, Robert Wood Johnson Medical School–University of Medicine and Dentistry of New Jersey, NJ 08854, USA.
R. J. Donnelly, Department of Lab Medicine and Pathology, New Jersey Medical School–University of Medicine and Dentistry of New Jersey, Newark, NJ 07103, USA.
R. K. Pullarkat, New York State Institute for Basic Research in Developmental Disabilities, Staten Island, NY 10314, USA.

*To whom correspondence should be addressed.